

©2016

Qi Qiao

ALL RIGHTS RESERVED

STRUCTURE AND CLUSTERING OF COLLOIDAL DIMERS ON A SURFACE

By

QI QIAO

A thesis submitted to the

Graduate School – New Brunswick

Rutgers, The State University of New Jersey

In partial fulfillment of the requirement

For the degree of

Master of Science

Graduate Program in Chemical and Biochemical Engineering

Written under the direction of

Dr. Yee C. Chiew

Dr. Meenakshi Dutt

And approved by

New Brunswick, New Jersey

May, 2016

ABSTRACT OF THE THESIS

STRUCTURE AND CLUSTERING OF COLLOIDAL DIMERS ON A SURFACE

By QI QIAO

Thesis Director:

Dr. Yee C. Chiew

Dr. Meenakshi Dutt

The study of two-dimensional (2D) structures formed by nanoparticles and colloidal particles has attracted a great deal of attention due to the rich and diverse structural patterns found in these systems. The self-assembly of particles into periodic phases is of relevance to technological applications in photonics, biomaterials, catalytic supports, and advanced materials. Very recently growing attention has been paid to the investigation of the self-organization of colloidal dumbbells, that is, dimers composed of two connected spherical particles. Because of the technical capability to synthesize dimeric nanoparticles of different sizes, aspect ratios, and asymmetric functionalizations, recent studies have demonstrated that these anisotropic particles exhibit diverse periodic structures and can be used as building blocks for the fabrication of new materials. We report an extensive study of the structure and clustering properties of colloidal dimers that interact through excluded-volume interactions combined with short-range attraction and long-range electrostatic repulsion. Such inter-particle interacting potential can generate particle aggregates through short-range attraction and cluster stabilization due to long-range repulsion. We carried out a systematic molecular dynamics simulations to study the behavior of colloidal dimers that interact through this potential on a two dimensional planar

surface. Using mathematic analysis of the radial distribution functions, cluster size distributions, and thermodynamic properties of the colloidal system, we have identified different distinct structural states: disordered fluids, finite-size aggregates, one-dimensional clusters, and percolating gel phase. At very low temperatures, the system may exist as a low-density ordered phase. We also examine the structure of the clusters, and the dynamics of the aggregation process. Our study enables us to map a phase diagram for the colloidal dimer system on the temperature-density plane. The information obtained in this study provides fundamental scientific insight and shed lights on the behavior of non-spherical colloidal dimers adsorbed on a planar surface.

ACKNOWLEDGEMENTS

My deepest gratitude goes first and foremost to my advisors, Dr. Yee C. Chiew and Dr. Meenakshi Dutt, for their constant encouragement, insightful guidance and great support that walked me through all the stages of the writing of this thesis and completed my research project.

Secondly, I'd like to take this opportunity to show my sincere gratitude to Abhinav S. Raman and Zeyu Yang. They helped me and provide me illuminating references and information about coding, algorithm and technical details for the simulation. This research would not have been possible without their invaluable advice, support and enormous patience throughout my graduate study at Rutgers University.

Furthermore, I would like to thank Dr. Nina Shapley for being my committee member and providing invaluable advice on my work.

Finally, I take this opportunity to convey my sincere thanks to my dear parents, my group members, and all of my friends who supported me in any respect during my M.S study.

TABLE OF CONTENTS

ABSTRACT OF THE THESIS	ii
ACKNOWLEDGEMENTS	iv
Chapter 1 Introduction	1
Chapter 2 Dumbbell Dimer system.....	5
2.1 Simulation Details	5
2.2 Description of the structural calculations and analysis	7
Chapter 3 Results and Discussion.....	9
3.1 Effect of the temperature.....	9
3.2 Effect of density	15
3.3 Mean Square Displacement and diffusion coefficient	20
3.4 Percolation Transition	23
3.5 Transitions and Dynamics	24
3.6 Effect of other factors.....	26
3.6.1 Monomer system	26
3.6.2 Cooling rate	27
Chapter 4 Conclusion.....	29
APPENDIX.....	31
.....	32
REFERENCES	33

Chapter 1 Introduction

The study of two-dimensional (2D) structures formed from nanoparticles and colloidal particles has attracted a great deal of interests due to the rich and diverse structural patterns found in these systems. The self-assembly of particles into periodic phases is of relevance to technological applications in photonics, biomaterials, catalytic supports, and advanced materials. Recent studies have shown that the patterns formed and structural transitions occurred depend strongly on the shape and strength of the inter-particle potentials between the colloidal particles [1, 2]. The competition between hard and soft repulsions can give rise to a rich variety of self-organized structures including stripes, lattices, cluster crystals and geometrically frustrated phases [3]. For example it has been found that a hard sphere-hard-shoulder purely repulsive potential, that contains of two characteristic length scales, forms stripe and ordered triangular structures [4]. Murari Singh and Hongjun Liu used Metropolis Monte Carlo simulations to obtain the structures, formed by square shoulder fluids with different shoulder widths, that yield different minimum energy structures and equilibrium phases [5-6]. Other studies have been devoted to interpreting structural phenomena such as jamming, melting and glass transitions of hard particle systems [7-13].

Very recently growing attention has been paid to the investigation of the self-organization of colloidal dumbbells, that is, dimers composed of two connected spherical particles. Because of the technical capability to synthesize dimeric nanoparticles of different sizes, aspect ratios, and asymmetric functionalizations, recent studies have demonstrated that these anisotropic particles exhibit diverse periodic structures and can be used as building blocks for the fabrication of new

materials [14-22]. Han and Kim discussed a 2D system with binary disks and snowman-shaped (called “snowman”) dimeric particles under short-range attraction. They found that a disorder-order transition exists depending on the strength of orientational correlation and concluded that attractive interactions does not significantly impact the structures formed [23]. They further showed that these asymmetric dumbbells (snowman dimers) formed complex structures including superlattices and glass phase at high densities that are not observed for monodisperse 2D spherical particles or disks [24].

Oliveira and E. Neves studied diatomic molecules interacting with a core-softened potential in three dimensions. They studied the effect of density on diffusivity and translational order parameter at constant temperature and identified the structural anomalies in the density-temperature and pressure-temperature phase planes. Additionally they found that dumbbell exhibits a much richer phase diagram than spherical monomeric particles [25, 26]. Recently, a broad range of investigations has been focused on the fabrication of non-spherical colloidal particles and their applications in drug delivery, molecular imaging and self-assembly [27]. In Daniel Salgado-Blanco and Carlos I. Mendoza’s work, they provided the self-assembly of core-cornu discs which interacted via anisotropic potentials in two dimensions and observed a numerical change of self-organized structures [28]. To better understand the behavior of the structural transitions, they then mapped out the phase diagram that showed the transition between disordered fluid phase and low-temperature ordered structures and provided various patterns in low-temperature arrangements [29].

In this thesis research, we are interested in studying dumbbell colloidal particles that interact through a strong short-ranged attraction coupled with a long-ranged

electrostatic repulsion. Particle clusters are formed as a result of the strong short ranged attraction. Because of the presence of long-ranged repulsion and the relatively deep attractive well, sufficient thermal energy is needed for a dumbbell to dissociate itself from a cluster. Hence, at low to moderate temperatures, the dumbbells are expected to form finite clusters and percolating gels. This competing short-range attraction and long-range electrostatic repulsion can also lead to dynamic arrested states studied by Zaccarelli and coworkers [30-38]. Dynamic arrest could be monitored by the calculation of mean square displacement and diffusion coefficient of the colloidal dumbbells [39-41].

In this work, we study colloidal dumbbells that interact through a potential that combines a Lennard-Jones with a Yukawa potential term (see Eq. (1) in chapter 2). This hybrid pair potential energy consists of excluded volume repulsion, short-range attraction, and long-range electrostatic repulsion. The competing short-range attraction and long-range repulsion can give rise to a wealth of patterns and structural transitions. The objectives of this thesis research are:

- (i) To investigate the self-organization and structural transitions of the proposed dumbbell model in two-dimension. This was achieved by performing a systematic and extensive molecular dynamics simulation over wide temperature and density ranges at constant N , V , and T conditions. The structures of the system were characterized by computing the spatial radial distribution function, static structure factors, cluster size distributions of the system, and mean square displacements (MSD).
- (ii) To examine the gelation (percolation) behavior and dynamics of arrest of the 2D dumbbells. Percolation probability and gelation transition of the

system were obtained as a function of temperature and density. The dynamics of arrest was determined by calculating the diffusion coefficient of the dumbbell colloids.

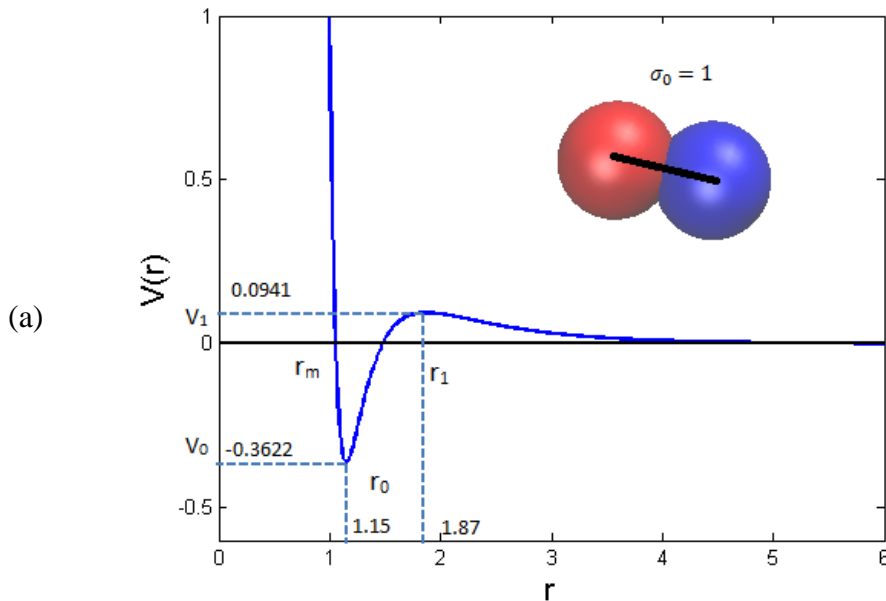
Chapter 2 Dumbbell Dimer system

2.1 Simulation Details

We consider a collection of colloidal dimers or dumbbells distributed in a 2D system at specified temperature and density. The two beads or particles in each dumbbell are connected by a fixed rigid bond of length $\sigma_0 = 1$. The beads or particles in different dumbbells interact with each other through hybrid potential composed of a Lennard-Jones potential and Yukawa term:

$$V(r) = 4\epsilon \left[\left(\frac{\sigma}{r} \right)^{12} - \left(\frac{\sigma}{r} \right)^6 \right] + A \frac{e^{-\kappa r}}{r} \quad (1)$$

In Eq. (1), ϵ is the depth of the potential well, σ represents the characteristic size of a bead at which the inter-particle potential is zero, and r is the separation between the particles. The parameter A is the amplitude of Yukawa potential and κ is another scaling constant that represents for screening length. For this hybrid potential we have $\sigma = 1$, $\epsilon = 1$, $r_0 = 1.15$, $\epsilon_0 = -0.3622$ and $r_1 = 1.87$ with $\epsilon_1 = 0.0941$. This potential model mimics a short range attraction (van der Waals or hydrophobic attraction) coupled to long-range electrostatic repulsion that are encountered in many colloidal systems.



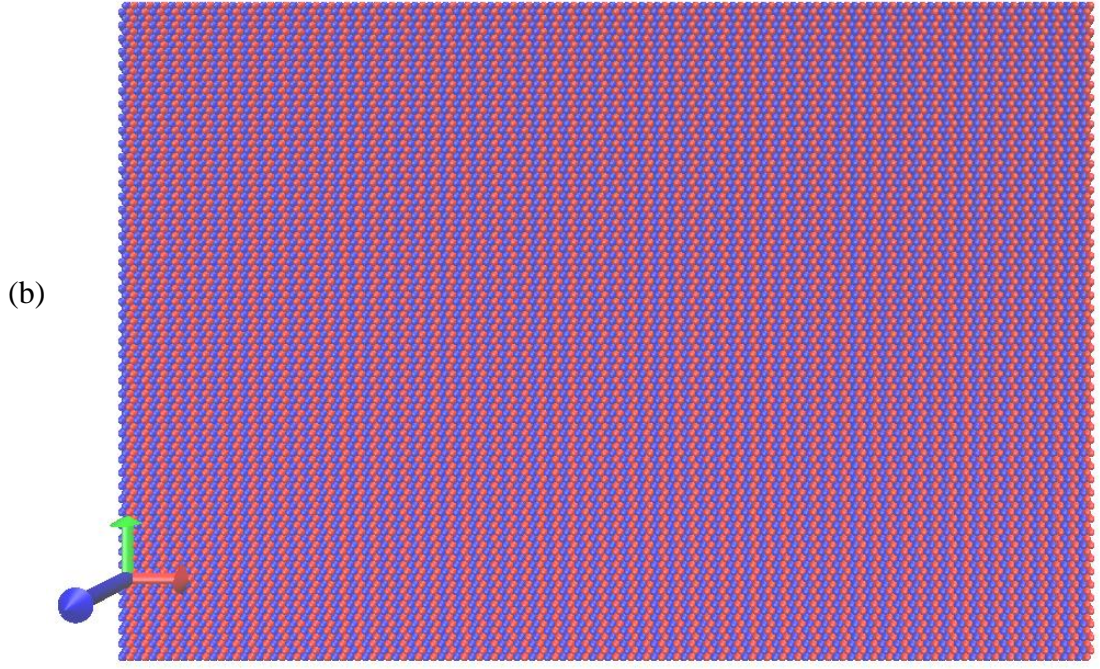


Figure 1. (a) The hybrid potential used in the simulation, where $\varepsilon = \sigma = \kappa = 1$, $A=2.25$ and the global cutoff for Yukawa interactions equals to 6, (b) Initial configuration of the colloidal dimer system.

Extensive molecular dynamic (MD) simulations were carried out for systems consisting of 6,400 dimers (or, 12,800 beads or particles) in canonical (NVT) ensemble at fixed values of density ρ and temperature T . For some thermodynamics states, a small number of runs were performed at constant pressure and temperature (NPT ensemble). Periodic boundary conditions in all directions are used. For all runs, an initial configuration comprising 6,400 well-ordered crystalline dimers is used. Each MD run begins by heating the dimeric crystal to $T^*=2.0$ until the dimers are randomly distribution within the 2D box subsequently the system is cooled down to the target temperature. The molecular dynamics simulation system is defined in terms of the following dimensionless quantities: temperature T^* , density ρ^* , pressure P^* , energy E^* , and time t^* :

$$T^* \equiv \frac{k_B T}{\varepsilon} \quad (2)$$

$$\rho^* \equiv \rho \sigma^2 \quad (3)$$

$$P^* \equiv \frac{P \sigma^3}{\varepsilon} \quad (4)$$

$$E^* \equiv \frac{E}{\varepsilon} \quad (5)$$

$$\tau^* \equiv \tau \sqrt{\frac{\varepsilon/m}{\sigma^2}} \quad (6)$$

Molecular dynamics runs were performed at temperatures ranging from $T^*=0.045$ to 2.00 over densities varying from 0.05 to 0.7. A time step of $\Delta t^* = 0.002$ is used in the MD simulations.

2.2 Description of the structural calculations and analysis

To quantify the spatial arrangements of the dimers, we obtain the radial distribution function which measures the local density of the dimers or beads. Two types of radial distribution functions are considered: the bead-bead radial distribution function $g_{aa}(r)$ which accounts for the probability of finding two spherical beads in two dimers that are separated by a distance r , and the dumbbell-dumbbell radial distribution function $g_{mm}(r)$ which measures the local density between the center-of-mass of a pair of dimers. The distribution functions are computed through the use of Eq. (7) where $n(r)$ represents the number of beads or molecules located within the shell between $(r - \Delta r)$ to r ,

$$g(r) = \frac{n(r)}{\pi(r^2 - (r - \Delta r)^2)} \quad (7)$$

The static structure factor $S(q)$ of the system can be calculated from the radial distribution functions through Eq. (8):

$$S(q) = 1 + 2\pi\rho \int_0^\infty r[g(r) - 1] J_0(qr) dr \quad (8)$$

where $J_0(z)$ represents the Bessel function of the first kind of order zero,

$$J_0(z) = \frac{1}{2\pi} \int_0^{2\pi} e^{iz \cos \theta} d\theta \quad (9)$$

In addition, we computed the cluster size distribution of the clusters formed at different temperature and density. The heat capacity (C_v) was calculated using the fluctuation formula

$$C_v = \frac{1}{Nk_B T^2} (\langle E^2 \rangle - \langle E \rangle^2) \quad (10)$$

To measure the dynamics of the system, we track the mean square displacement (MSD) of the dimers and calculate the diffusion coefficient (D) through the relation given below:

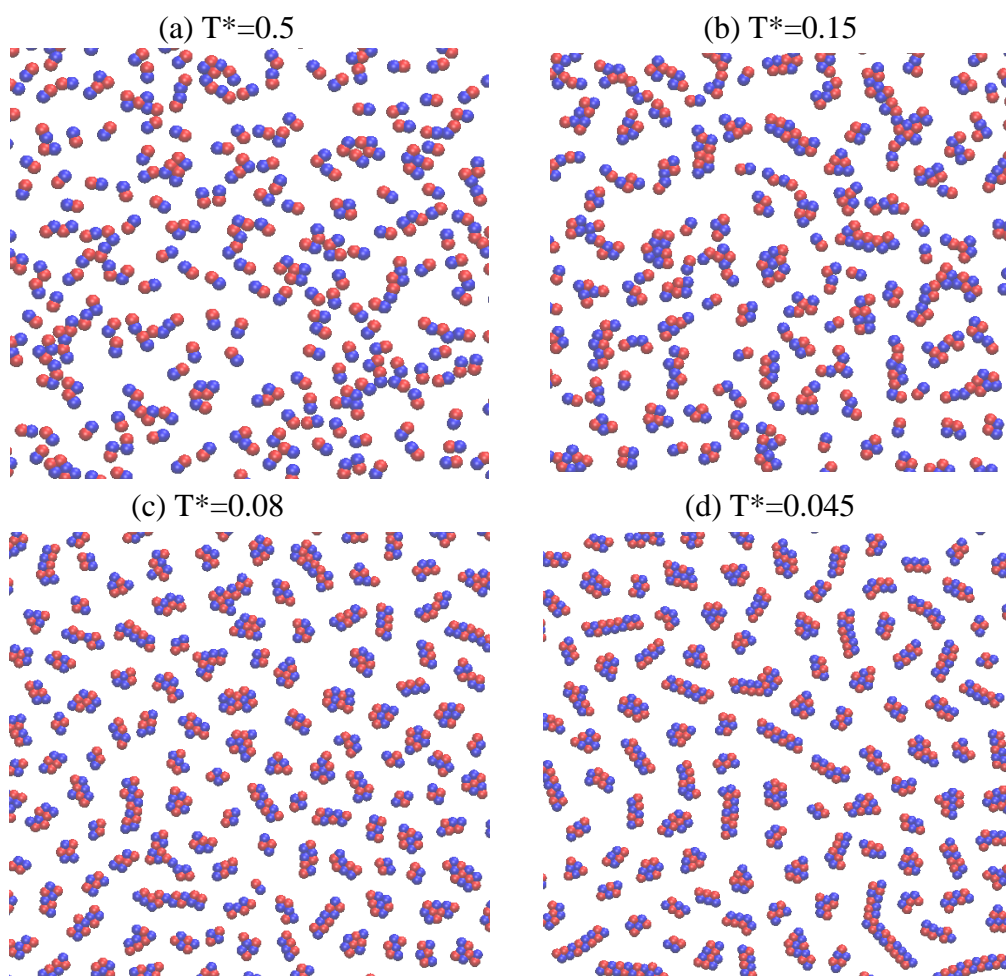
$$MSD \equiv \langle (x(t) - x_0)^2 \rangle = 4Dt \quad (11)$$

Chapter 3 Results and Discussion

In this chapter, we report analysis of results and new findings obtained from our extensive and systematic molecular dynamics. It is found that the 2D system exhibits rich and diverse self-organized structure and patterns. We shall examine the effects of temperature on the clustering structures, followed by the effect of density. These results are presented in the following sections.

3.1 Effect of the temperature

Figure 2 displays representative snapshots of the dimer configurations at $\rho^*=0.204$. from $T^*=0.5$ to $T^*=0.008$. Five distinct patterns are observed as temperature is decreased.



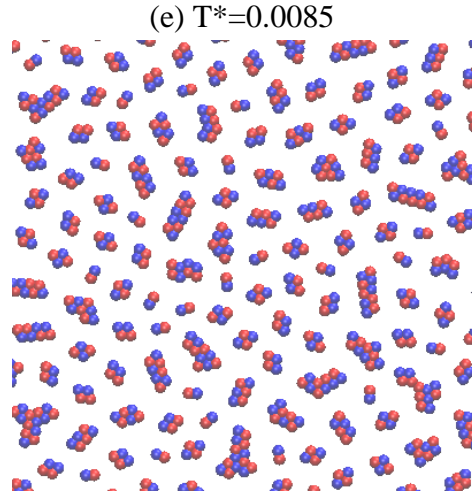
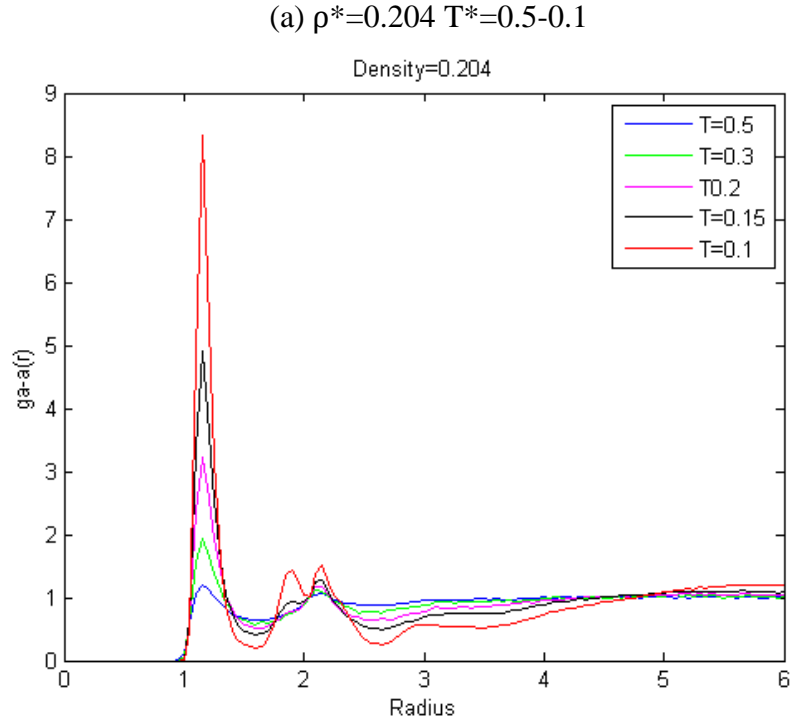


Figure 2. Visual images of structures at $\rho^*=0.204$ of different temperatures for NVT system. (a) shows $T^*=0.5$, (b) shows $T^*=0.15$, (c) shows $T^*=0.08$, (d) shows $T^*=0.045$, (e) shows $T^*=0.0085$.

Figure 2(a) shows that at high temperature $T^*=0.5$, the system adopts a disordered structure. As temperature decreases to $T^*=0.15$, the dimers start to form small “open” clusters as illustrated in Figure 2(b). At $T^*=0.08$, the clusters become more compact and the dimers are well-ordered within each cluster. As temperature decreases to $T^*=0.045$, the clusters grow to form short filaments, as shown in Figure 2(d).



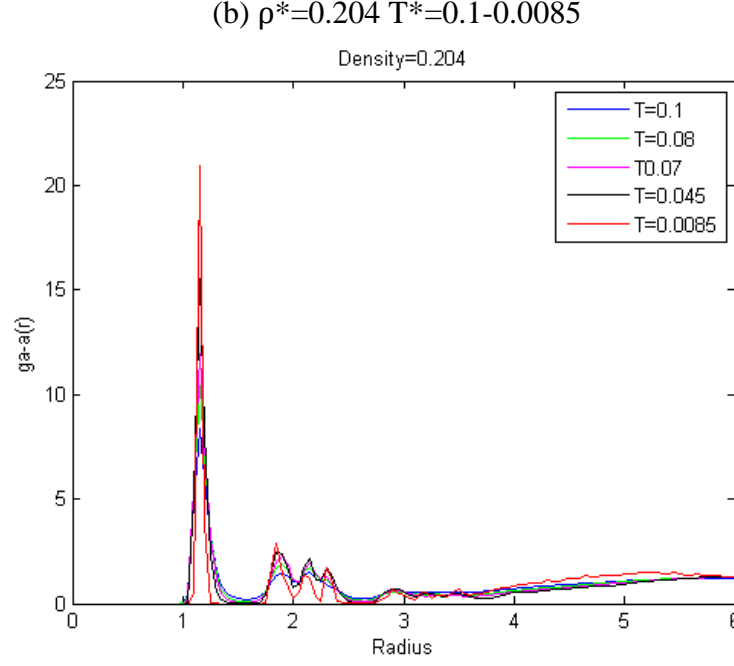


Figure 3. Structural properties at $\rho^*=0.204$ NVT system. (a) Radial distribution functions $g_{aa}(r)$ for the distance between atoms at high temperature $T^*=0.5-0.1$. (b) Radial distribution functions $g_{aa}(r)$ for the distance between atoms at low temperature $T^*=0.1-0.0085$.

We have computed the bead-bead radial distribution function $g_{aa}(r)$ and the dimer-dimer distribution function $g_{mm}(r)$. The function $g_{aa}(r)$ represents the probability of finding two beads (“atoms”) in two different dimers, separated by a distance r , while $g_{mm}(r)$ accounts for the probability of finding two dimers based on their center-of-mass. Careful analysis of the distribution functions in Figure 3 reveals that these functions provide a quantitative description of the structure of the clusters described above. Figure 3(a) shows that for $T^*>0.15$, the function $g_{aa}(r)$ possesses a peak at $r \sim 1.15$, and a second peak at $r \sim 2.15$. These features indicate that, at these temperatures, the dimers form small clusters that are “loose” and disordered as described in Table 1 (first row). The peak positions at $r=1.15$ and 2.15 correspond to linear or T-shaped clusters depicted in the Table. At $T^*=0.15$, a set of double peaks emerges at $r \sim 1.85$ and 2.15 which suggests that the clusters become more compact and the dimers within the clusters adopt ordered arrangements as illustrated in Table 1

(second row). Note that the double peak positions correspond to the clusters shown in the Table.

Table 1. The analysis of peak positions in $g_{aa}(r)$ and its specific structures.

T^*	Average Cluster size/molecule	Peak information in $g_{aa}(r)$	Visual image
0.3	2	Two peaks	
0.15	3	Emergence of Double peak	
0.045	4	Emergence of Triple peak	

At $T^*=0.08$ and 0.045 , the dimers formed small compact clusters (Figure 2(c) and 2(d)). Representative snapshots of the system show that the dimers have a tendency to grow in a lengthwise direction into short filaments even though a small number of the clusters are “non-linear” in shape. Within each cluster or filament, the beads of the dimers are arranged in an ordered structure, with a “ filament thickness” of two

beads wide. These “two-bead thick” filaments are characterized by a set of triple-peaks at $r \sim 1.85, 2.15$ and 2.30 in the radial distribution function $g_{aa}(r)$ as shown in Figure 2(a). The structure of these filaments and their corresponding peak positions are illustrated in Table 1. In these structures, the dumbbells take up configurational arrangements that minimize the energy of the system. Also, the clusters exist as distinct islands prevented from coalescing with each other by the long-range repulsion between the beads. At $T^*=0.0085$, the clusters (of varying shapes and sizes) appear to form imperfect defective hexagonal lattice.

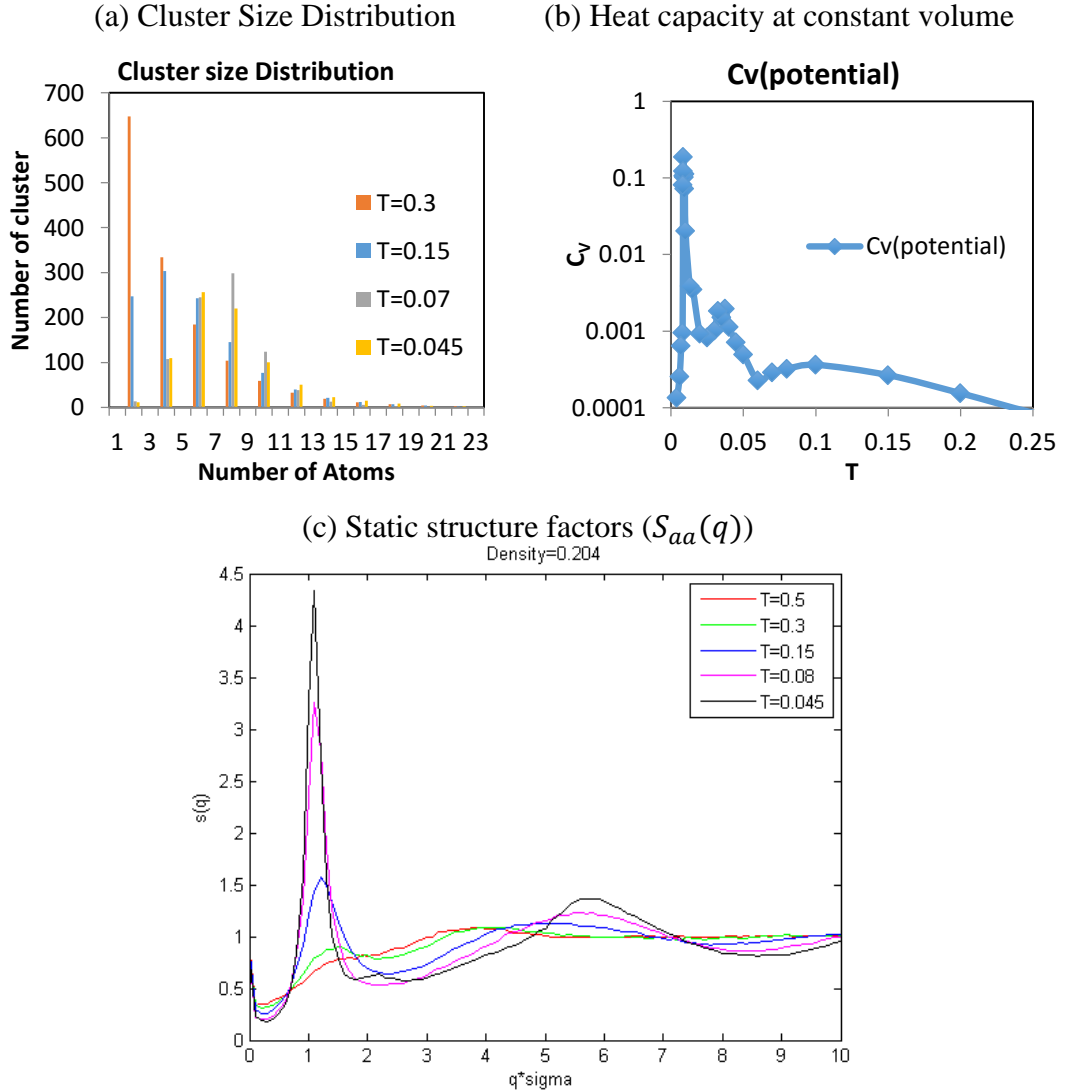


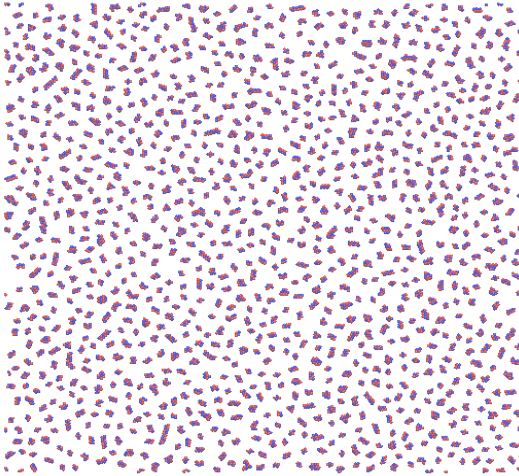
Figure 4. Structural properties at $\rho^*=0.204$ NVT system. (a) Cluster size distributions for special temperature that shown different patterns. (b) Potential heat capacity at constant volume. (c) Static structure factors $S_{aa}(q)$ for $\rho^*=0.204$ NVT system.

Figure 4(a) presents the size distributions of the clusters formed at $\rho^*=0.204$ and at different temperatures. Plotted are the numbers of clusters versus the size (number of beads) of the cluster. The smallest cluster is simply a dimer consisting of 2 beads. It is seen that at $T^*=0.3$, there is a large number of non-aggregated dumbbells. As temperature is decreased, the size distribution shifts to large cluster. The dimer system undergoes several structural transitions which are reflected in the peaks of the constant volume heat capacity C_V at $T^*=0.1$, $T^*=0.0375$ and $T^*=0.0085$ as shown in Figure 4(b). The first peak in C_V represents the commencement to form well-ordered pattern around $T^*=0.1$ to $T^*=0.15$. Second peak exhibits the formation of one-dimensional long clusters between $T^*=0.0375$ and $T^*=0.045$, and the third peak corresponding to the hexagonal-latticed structure in the system at $T^*\sim 0.0085$. The static structure factors $S_{aa}(q)$ shows that the emergence of first peak between $T^*=0.3$ and $T^*=0.15$, which means there is a phase transition from disordered patterns to an ordered structure.

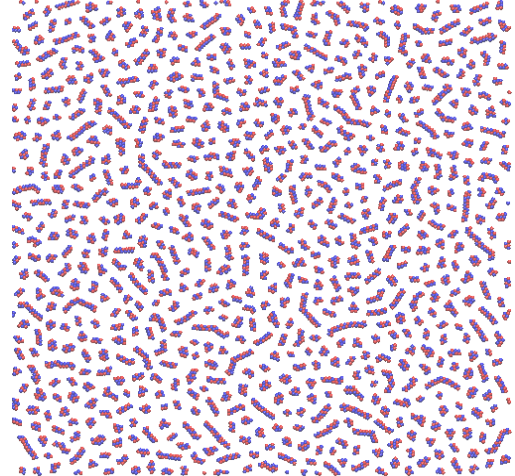
3.2 Effect of density

In this section we examine the effect of density on the clustering behavior of the dumbbells. As density increases the average separation between the dimers decreases; the competitive interaction between the short-range attraction and long-range repulsion leads to interesting clustering patterns. Figure 5(a)-(f) show representative snapshots of the dimer configurations at $T^*=0.045$ at densities ranging from 0.142 to 0.70. At a low density of $\rho^*=0.142$, small clusters are formed (see Figure 5(a)). The bead-bead radial distribution function $g_{aa}(r)$ possesses a sharp peak at $r=1.15$, a set of triple peaks at $r \sim 1.85, 2.15$ and 2.85 , and $g_{aa}(r) = 0$ for $1.4 < r < 1.7$; these features are indicative of the formation of clusters consisting of two well-ordered dimers.

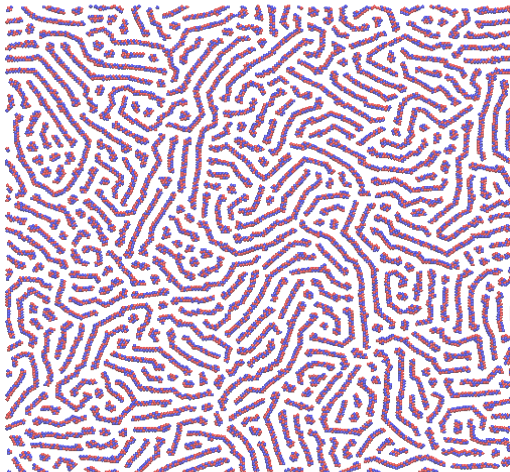
(a) $\rho^*=0.142, T^*=0.045$



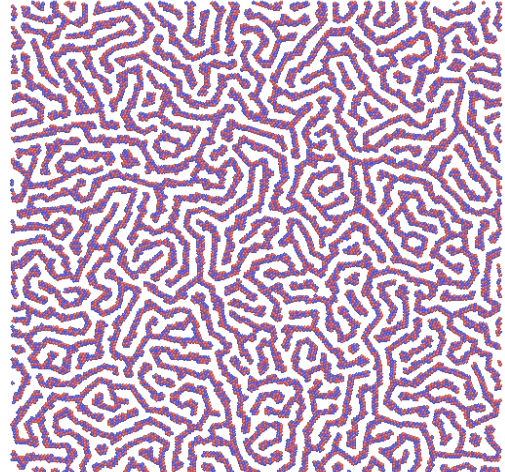
(b) $\rho^*=0.204, T^*=0.045$



(c) $\rho^*=0.318, T^*=0.045$



(d) $\rho^*=0.4, T^*=0.045$



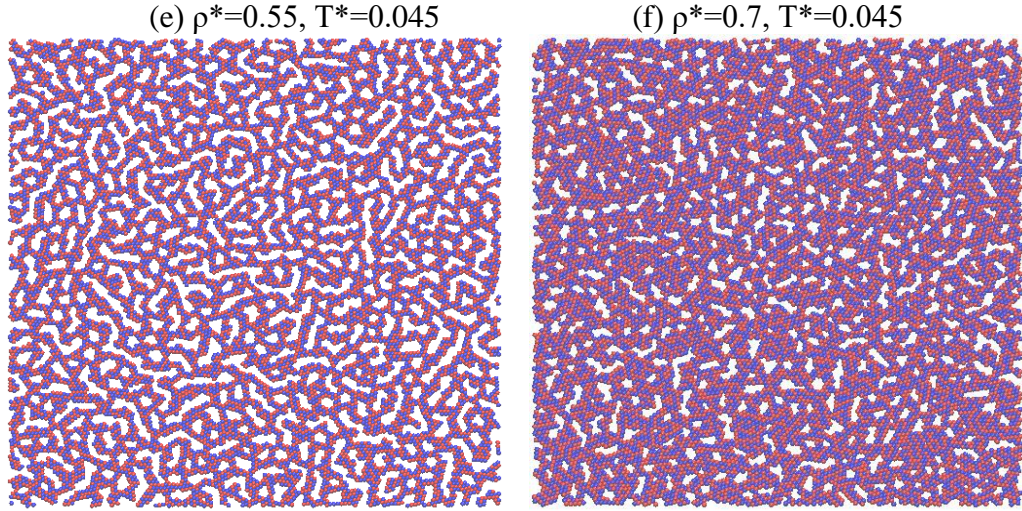


Figure 5. Configurational information about various densities. (a) $\rho^*=0.142$, $T^*=0.045$ NVT system. (b) $\rho^*=0.204$, $T^*=0.045$ NVT system. (c) $\rho^*=0.318$, $T^*=0.045$ NVT system. (d) $\rho^*=0.4$, $T^*=0.045$ NVT system. (e) $\rho^*=0.55$, $T^*=0.045$ NVT system. (f) $\rho^*=0.7$, $T^*=0.045$ NVT system, respectively.

It is further noted that the $g_{aa}(r)=0$ or much less than unity for $2.5 < r < 6.0$ suggesting that dimers are depleted at these separations owing to the long-range repulsion between the beads or particles that prevents clusters from coalescing with each other. Figure 5(b) shows that the clusters grow in length to form short filaments at $\rho^*=0.204$. At $\rho^*=0.318$, these clusters grow in a lengthwise direction to form long filaments. Typically they are two-bead wide and are prevented from aggregating nearby filaments by the long-range repulsion. These filaments grow in size and thickness and form branches at $\rho^*=0.4$. Figure 5(e) and 5(f) show that the dimers form a percolating cluster at $\rho^*=0.55$ and higher.

Figure 6 illustrates representative snapshots of the dimer configurations at $T^*=0.0085$ at $\rho^*=0.204$ and 0.318 . At this low temperature, the system consists of small clusters of varying sizes and short filaments. At this temperature, the clusters (not the dimers or beads) form crystalline hexagonal structure. The lattice structure is defective and imperfect partly because of the clusters of different sizes are situated at the lattice

points creating defects in the lattice structure (see Figure 5(e)). At $\rho^*=0.318$ and 0.4, the system becomes disorder and the clusters grow in size.

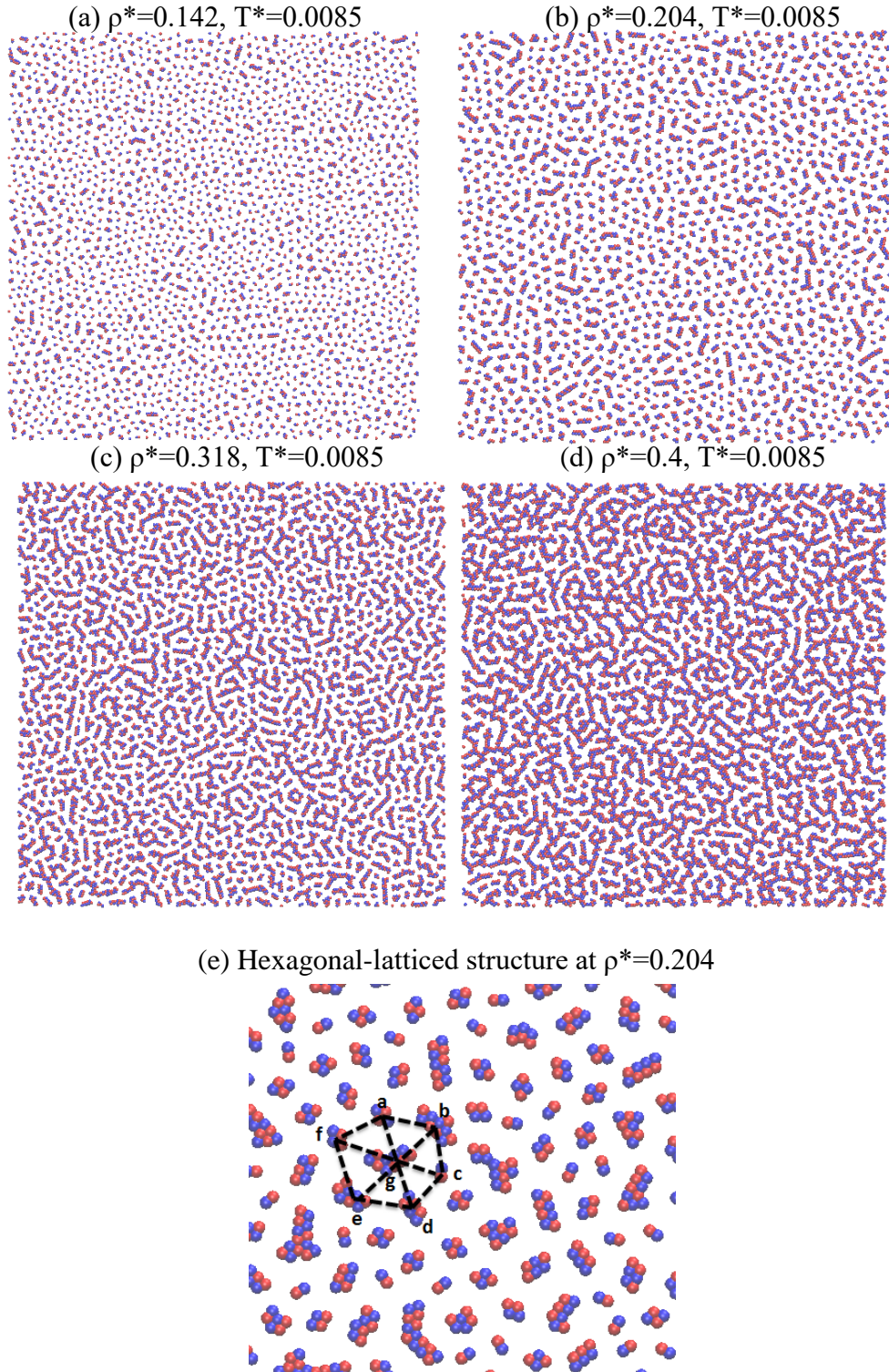
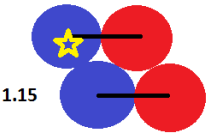
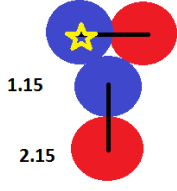
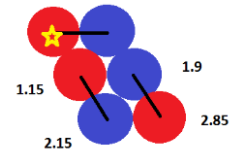
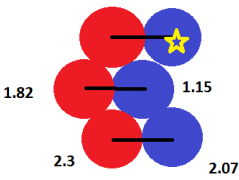
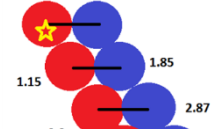
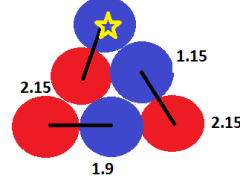
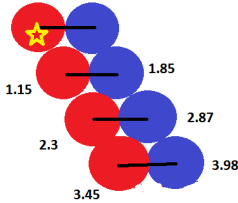
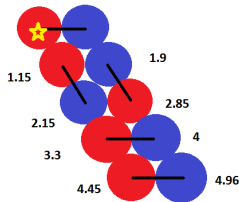


Figure 6. (a) Visual image of structure at $\rho^*=0.142$, $T^*=0.0085$ NVT system. (b) Visual image of structure at $\rho^*=0.204$, $T^*=0.0085$ NVT system. (c) Visual image of structure at $\rho^*=0.318$, $T^*=0.0085$ NVT system. (d) Visual image of structure at $\rho^*=0.4$, $T^*=0.0085$ NVT system. (e) Hexagonal-latticed structure at $\rho=0.204$, $T^*=0.0085$ NVT system

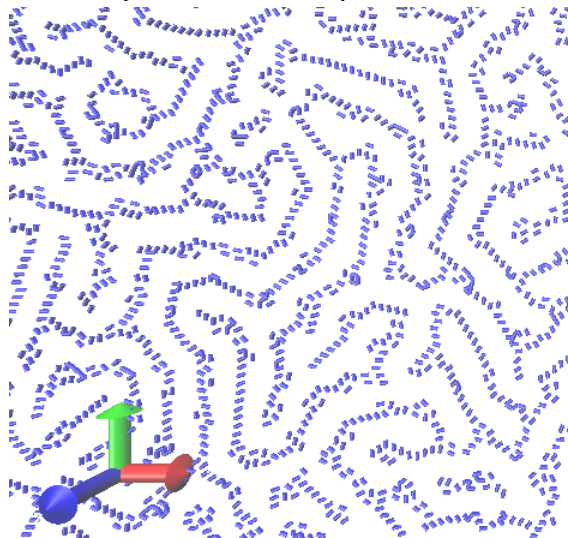
Table 2. The configurations and the correlative energy.

Peak positions and Energy			
Visual images	Energy	Visual images	Energy
(a)	R=1.15, E=-0.36218 R=1.85, E=0.093946 1 long 3 short E*=-0.992594	(b)	R=1.15, E=-0.36218 R=2.15, E=0.081814 2 long 2 short E*=0.560732
			
(c)	R=1.15, E=-0.36218 R=1.9, E=0.093905 R=2.15, E=0.081814 R=2.85, E=0.038216 6 long 6 short E*=-1.68948	(d)	R=1.15, E=-0.36218 R=1.85, E=0.093946 R=2.07, E=0.086961 R=2.3, E=0.071241 6 long 6 short E*=-1.668784
			
(e)	R=1.15, E=-0.36218 R=1.85, E=0.093946 R=2.07, E=0.086961 R=2.3, E=0.071241 R=2.87, E=0.037306 6 long 6 short E=-1.718439	(f)	R=1.15, E=-0.36218 R=1.85, E=0.093946 R=1.9, E=0.093905 R=2.15, E=0.081814 6 long 6 short E=-1.645841
			
(g)	R=1.15, E=-0.36218 R=1.85, E=0.093946 R=2.07, E=0.086961 R=2.3, E=0.071241 R=2.87, E=0.037306 R=3.14, E=0.026846 R=3.45, E=0.018333 R=3.98, E=0.009557 15 long 9 short E*=-2.384748	(h)	R=1.15, E=-0.36218 R=1.85, E=0.093946 R=1.9, E=0.093905 R=2.15, E=0.081814 R=2.3, E=0.071241 R=2.85, E=0.038216 R=3.0, E=0.031861 R=3.3, E=0.022053 R=3.65, E=0.014331 R=4.0, E=0.009326 R=4.11, E=0.008153 R=4.45, E=0.00539 R=4.96, E=0.002913 28 long 9 short E*=-1.93785
			

The MD simulations have illustrated that the system has a propensity to form linear filament-like clusters or stripes that grow in a preferred lengthwise direction. The dimers tend to arrange themselves to minimize its energy. We have carried out a detailed analysis of the configurational energy of ordered clusters of varying shapes and sizes. These results are displayed in Table 2. For clusters consisting of three dimers (rows 2 and 3 in Table 2), it is seen that filament-like clusters (c,d, e) have lower configurational energy than non-filament shaped cluster (f). Also, linear clusters made up of perfectly stacked dimers (e and g) tend to have the lowest energy (compare c, d, e and f).

Figure 7(a) illustrates clearly the tendency of the dimers to form uni-directional linearly arranged filaments that correspond to favorable low energy states. These linear unidirectional filaments are manifested in the triple-peaks that appeared in the bead-bead radial distribution function, as shown in Figure 7(d). Multiple sets of triple peaks are observed and they correspond to the linear clusters shown in Figure 7(b) and 7(c). These low energy filament structures persist at higher densities of $\rho^*=0.318$ and 0.40 even though the clusters are branched.

(a) Dynamic bonds at $\rho^*=0.4$, $T^*=0.045$



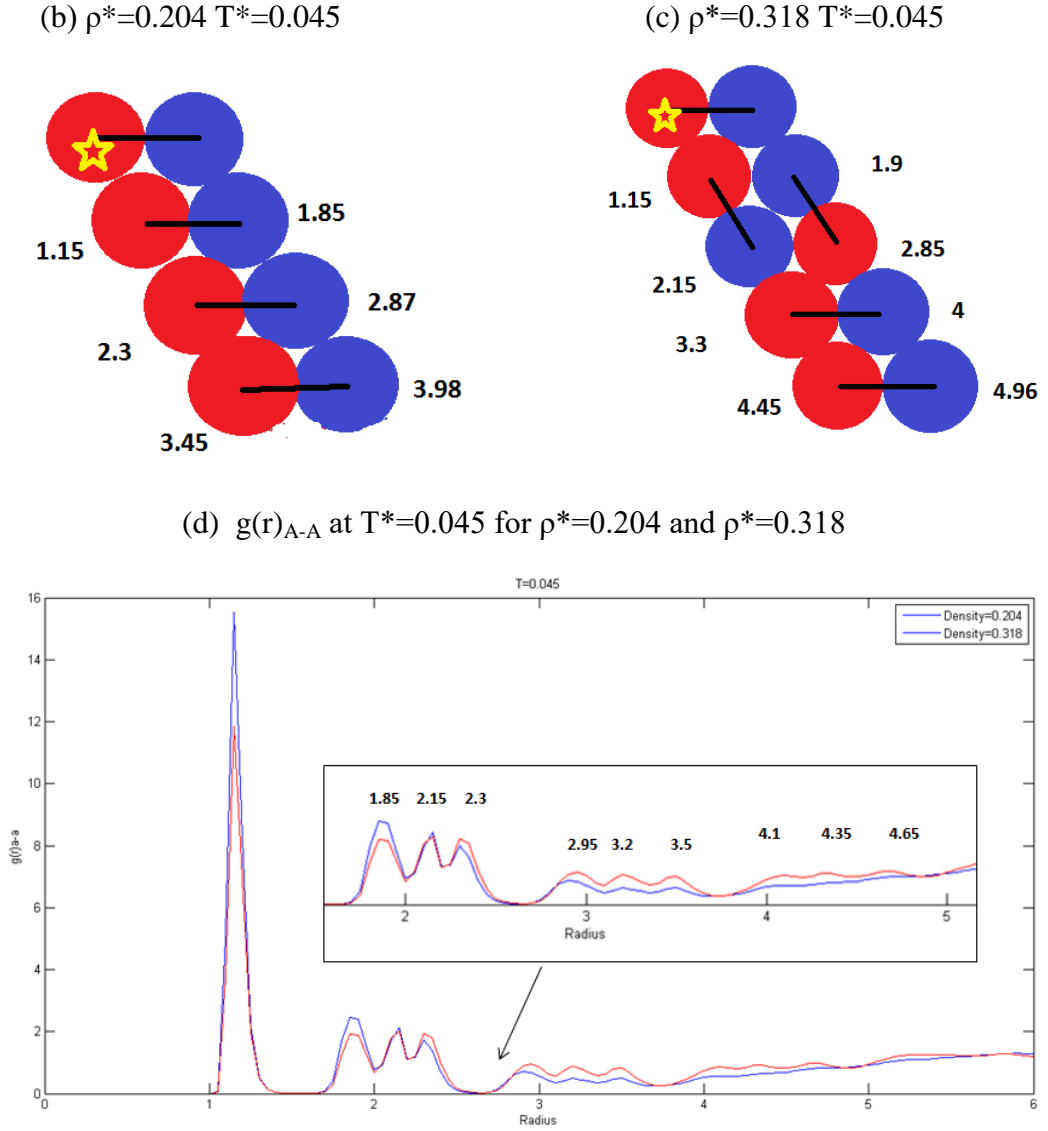


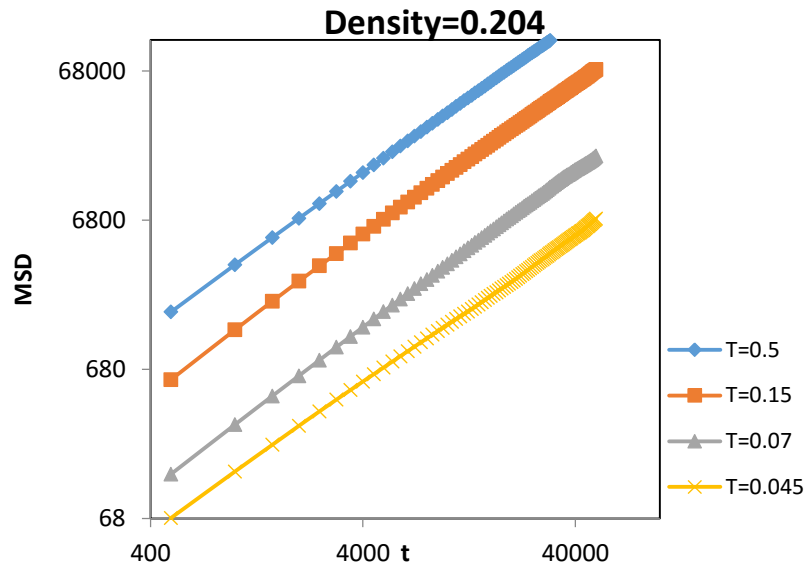
Figure 7. Specific pattern properties to analyze the shape of the structures. (a) Dynamic bonds to show the orders of the patterns at $\rho^*=0.4$ $T^*=0.045$. (b) Typical structure at $\rho^*=0.204$ $T^*=0.045$. (c) Typical structure at $\rho^*=0.318$ $T^*=0.045$. (d) $g_{aa}(r)$ at $T^*=0.045$ for $\rho^*=0.204$ and $\rho^*=0.318$ to show the emergence of more triple peaks.

3.3 Mean Square Displacement and diffusion coefficient

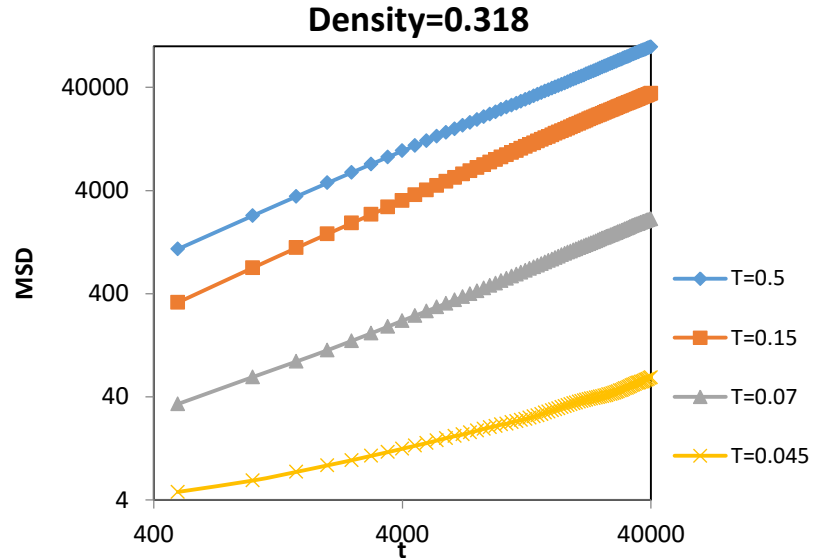
In addition to analyzing the configurational structure of the clusters form, we examine the dynamical and diffusional behavior of the system. Owing to the strong short

attractive well of the pair-potential energy (Figure 1(a)), dimers that are located in the well must possess sufficient thermal energy to escape it. Therefore, at low temperatures, the dimers may be dynamically arrested and are unable to overcome the attractive energy between them. When the dimers are dynamically arrested, one expects the diffusional process to deviate from Fickian behavior.

(a) MSD at $\rho^*=0.204$ $T^*=0.5, 0.15, 0.07$ and 0.045



(b) MSD at $\rho^*=0.318$ $T^*=0.5, 0.15, 0.07$ and 0.045



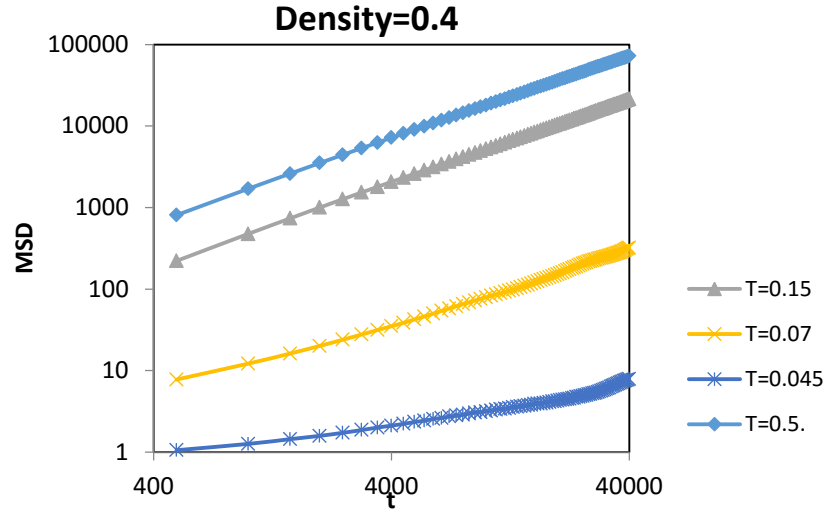
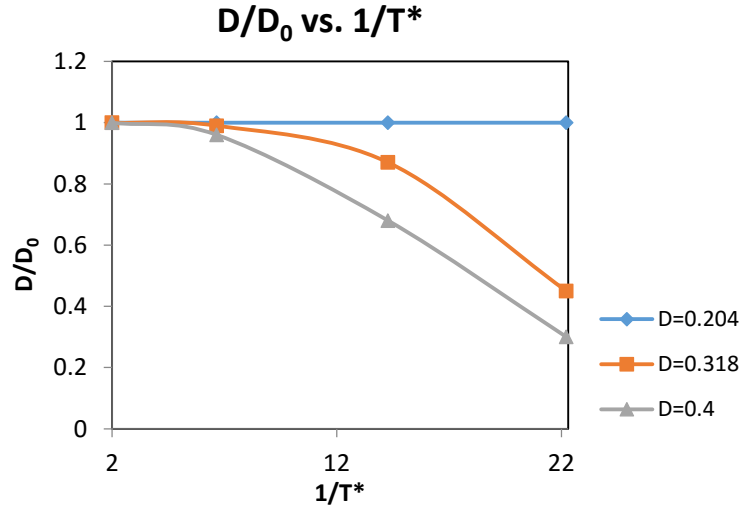
(c) MSD at $\rho^*=0.4$ $T^*=0.5, 0.15, 0.07$ and 0.045 (d) D/D_0 vs. T 

Figure 8. Mean square displacement (MSD) vs. time at $\rho^*=0.204, 0.318, 0.4$ with $T^*=0.5, 0.15, 0.07, 0.045$. And D/D_0 vs. $1/T^*$ has been shown as D calculated as diffusion coefficient.

We performed a series of simulations to track the mean square displacements of the dimers as a function temperature and density. We computed the mean square displacement (MSD) and the diffusion coefficient of the dimers via the well-known relation $D = \langle (X_t - X_0)^2 \rangle / 4t$. For Fickian diffusion, the slope of the MSD vs time curve is expected to be unity on a log-log plot. Figure 8(a) shows MSD vs t at $\rho^*=0.204$ at four different temperatures. The MSD follows a straight line behavior with a slope of unity implying Fickian diffusion behavior.

As density increases to $\rho^*=0.318$, the slope of MSD vs time curve falls below unity at T^* below 0.07 suggesting that the diffusion is sub-Fickian (Figure 8(b)). Similar trend is observed for $\rho^*=0.40$. This behavior is summarized in Figure 8(d) where we have plotted D/D_0 vs. $1/T$ where D_0 represents Fickian diffusion coefficient. It is evident from Figure 8(d) that non-Fickian diffusion occurs at low temperature and high density.

3.4 Percolation Transition

As density increases above $\rho^*>0.55$, visual image shows that one-dimensional structure disappears and clusters become “fatter.”

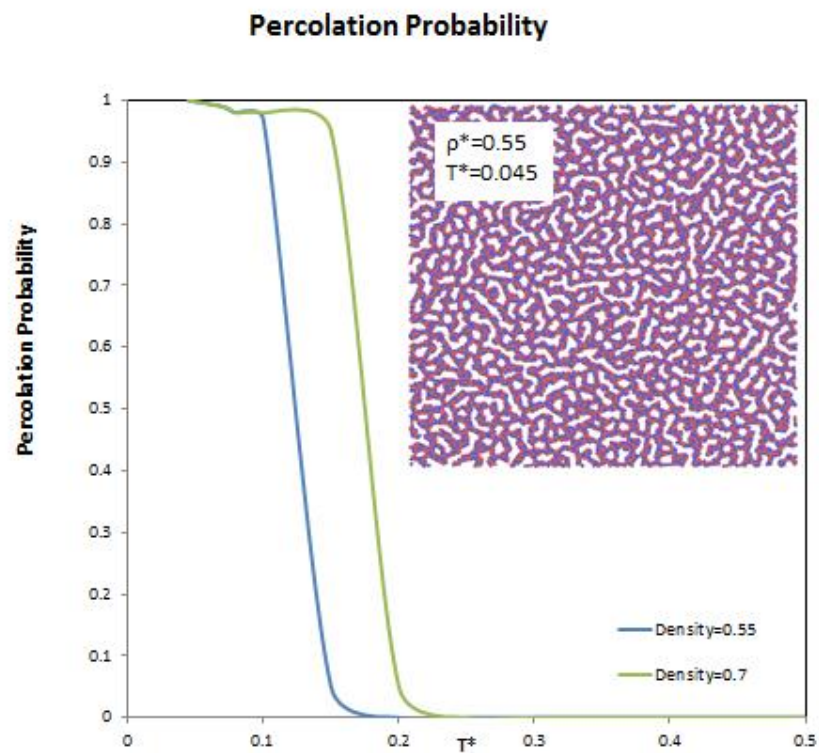


Figure 9 Percolating Probability and percolating gel phase structure at $\rho^*=0.55$ $T^*=0.045$.

Figure 9 show that at high density the clusters and small aggregates will connect together to form percolating network. We calculated the percolating probability at two densities $\rho^*=0.55$ and $\rho^*=0.7$. The percolating probability increases drastically from 0 to 1 in the vicinity of the percolation threshold as temperature is decreased from $T^*=0.15$ to $T^*=0.08$ at $\rho^*=0.55$. At a the high density $\rho^*=0.7$ the percolation transition occurs at higher temperatures $T^*=0.2$ to $T^*=0.15$.

3.5 Transitions and Dynamics

We plot the phase diagram based on our analysis of the structural properties of the configurations. For all the densities considered, we found that at temperature above $T^*=0.2$, the system exists as a disordered phase consisting of individual dimers or small clusters that have open structures (end-to-end or T-shape clusters). At temperatures between 0.1 and 0.15, there is a significant change of structural configurations whereby the dimers start to form well-ordered structures. This structural transition is also manifested as peaks in the heat capacity vs temperature plot. At lower temperatures, difference appears in different densities. Below $T^*=0.1$ is the ordered arrangements region, where the system will show several interesting specific patterns. All the dimers are well-placed and change from small finite-size aggregates, one-dimensional long stripes, percolating network to a gel phase as figures 7 are present. A structural transformation occurred when temperature reached $T^*=0.0085$, almost all the dimers and small crystals formed analogously hexagonal-latticed structure when density varied from $\rho^*=0.05$ to $\rho^*=0.204$. Because of the big difference of cluster size for each crystal, no distinct hexagonal arrangement existed at $\rho^*=0.318$ and $\rho^*=0.4$. For higher density like $\rho^*=0.55$ and above, the system

exhibited gel structures below $T^*=0.15$. And there is not an exactly defined line between different areas since the possibility of the coexistence regions.

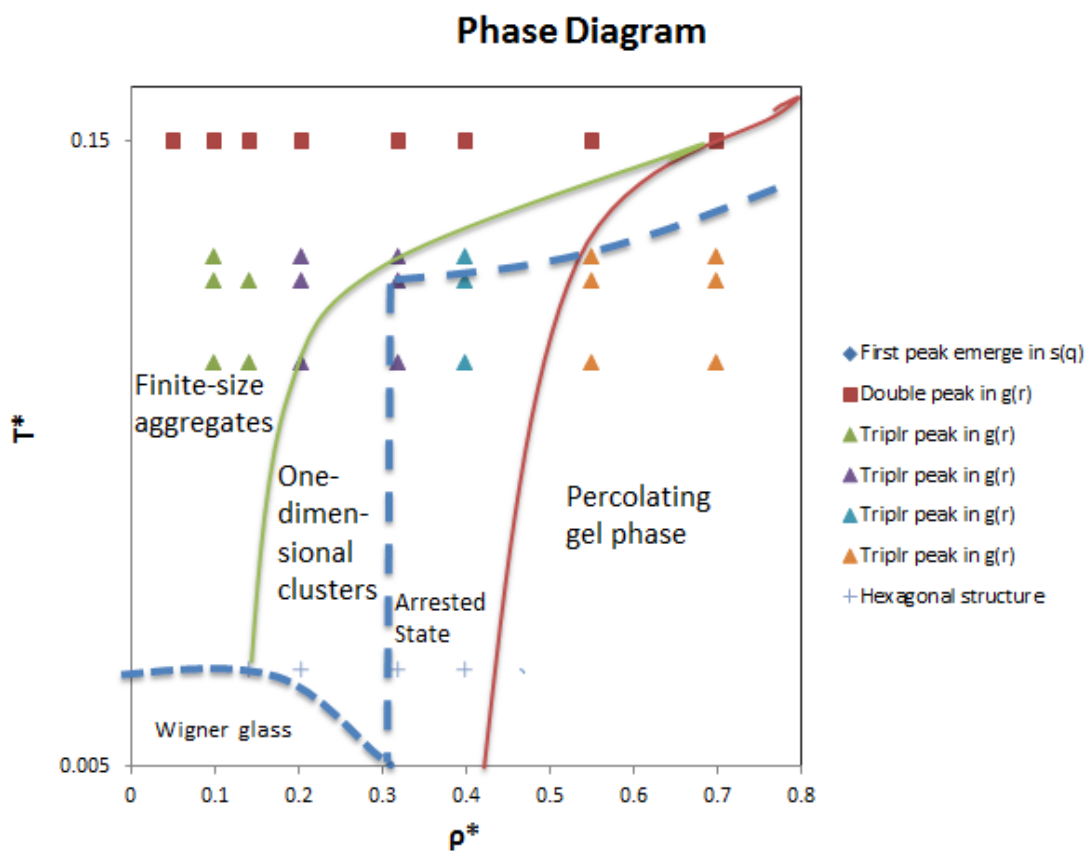
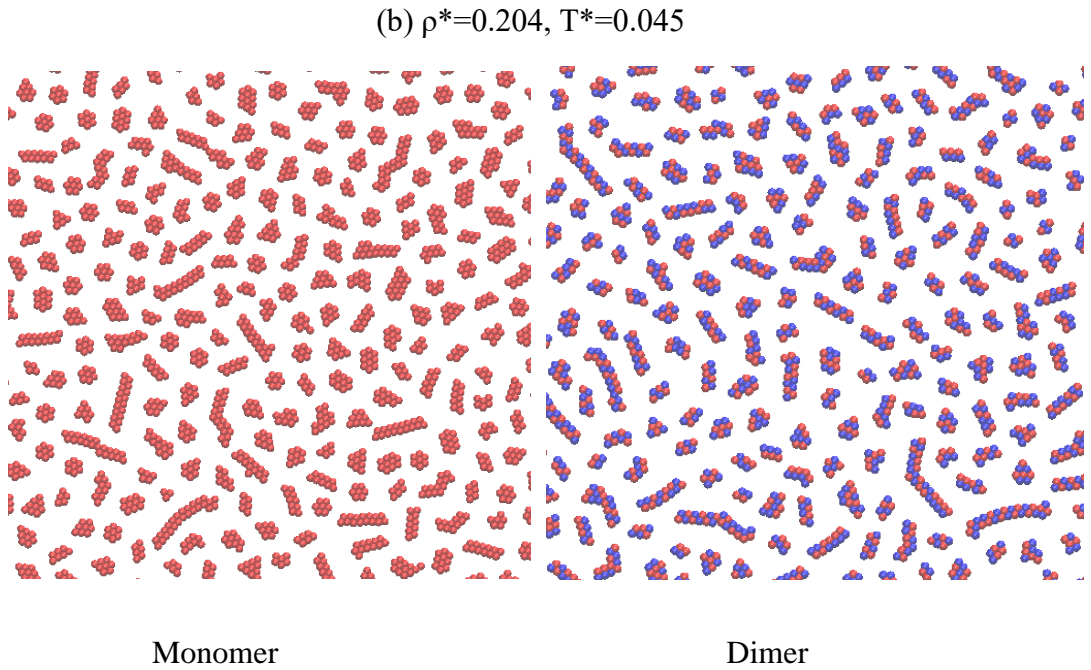
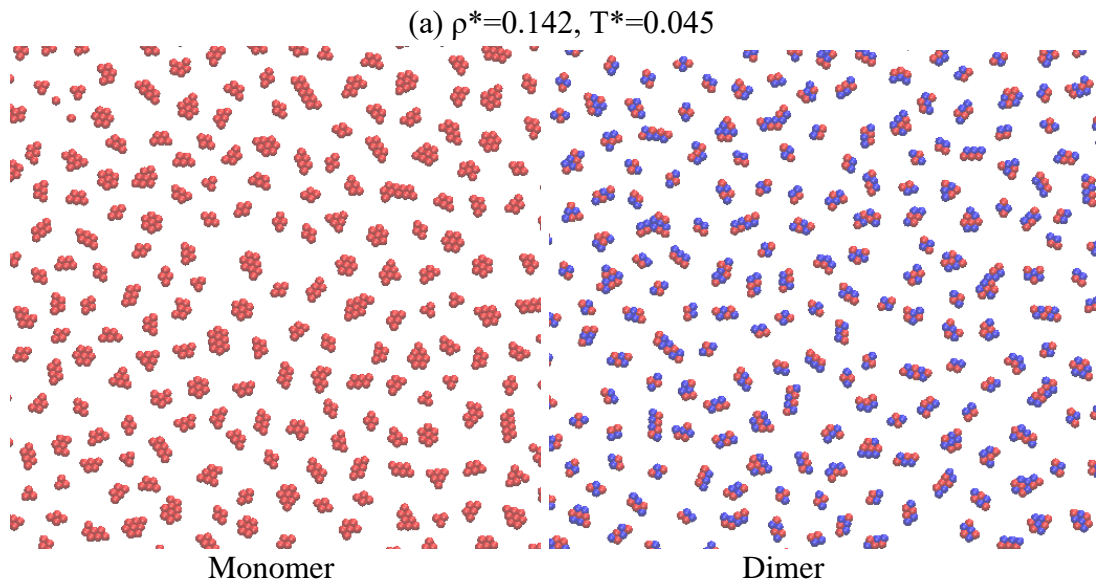


Figure 10. Phase Diagram, shown only well-ordered structures regions. The solid lines are adjusted by $g(r)$, $S(q)$ and static structure factors. Dash lines are drawn by MSD and diffusion coefficients data, to show the arrested stat region in the high density and low temperature areas and hexagonal-latticed structure in low temperature and low density parts as well.

3.6 Effect of other factors

3.6.1 Monomer system

We found many specific structures that dimers will form at different temperatures and densities, but there is one possibility that we could consider the one-dimensional long cluster pattern may be the effect of the bond between the two atoms. Therefore, we set up a monomer system that has the same conditions as the dimer system and run the simulations for several typical temperatures to compare the configurations.



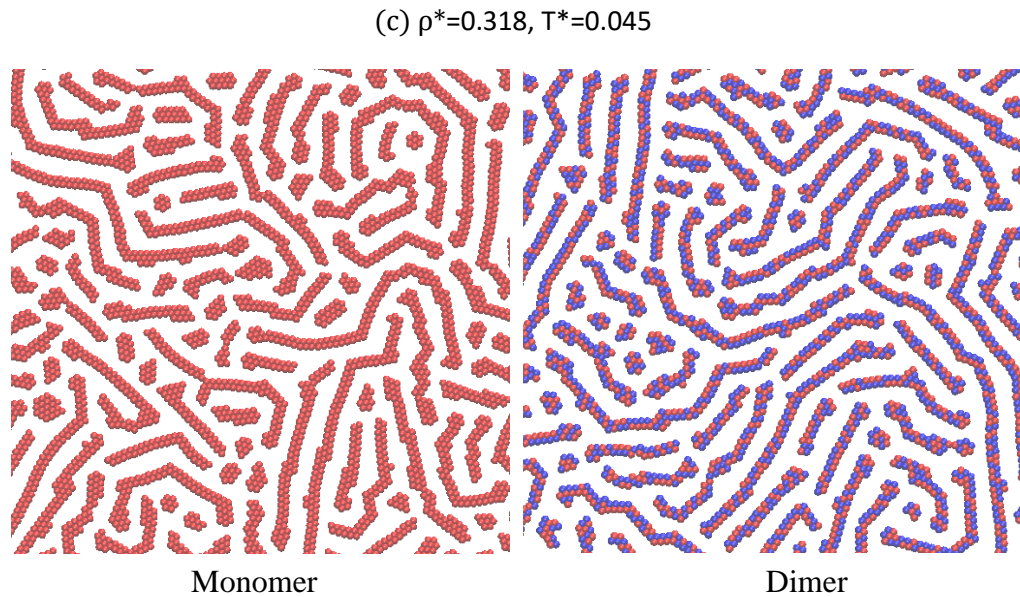


Figure 11. Configurations for monomers and dimers at same conditions. (a) At low density $\rho^*=0.142, T^*=0.045$, NVT system. (b) $\rho^*=0.204, T^*=0.045$, NVT system. (c) $\rho^*=0.318, T^*=0.045$, NVT system.

We repeated all the simulations we had done in dimer system at the exactly same conditions, and then show some special points that have specific structures to represent the results. In Figure 11 we could found that the bond which holds the dimer together doesn't affect the formation of the patterns in NVT system. After comparing $g(r)$ and cluster size distributions, we found that results are the same. More one-dimensional long clusters will be formed by dimers as density increases, and the same situation also occurred in monomer simulations. All these results show that the monomer system is identical to the dimer system.

3.6.2 Cooling rate

Considering there will be other factors that may have an effect on the structural formation, we designed another NVT system with various velocities and cooling rate at the same whole time step, reaction temperature and density. Meanwhile, we also set

up NPT system via using the average pressure in NVT system. Results shown that for different velocity, the system is categorically identical. Compared with structural properties of NVT and NPT system, only in some conditions NPT system could exhibit different results from NVT system. Due to limit density and temperature, it is difficult for us to figure out the discipline of the difference between NVT and NPT system. And for cooling rate, however, has a huge impact on both NVT and NPT system. The system will show a different cluster size distribution since we change the cooling rate. It is possible that the cooling rate may have an effect on catalyzing or destroying the dynamic arrested states and forces the system to find another available localization length and results in various cluster size change. These results suggested another way to further discuss about this research. The whole process is shown as blew in figure 12.

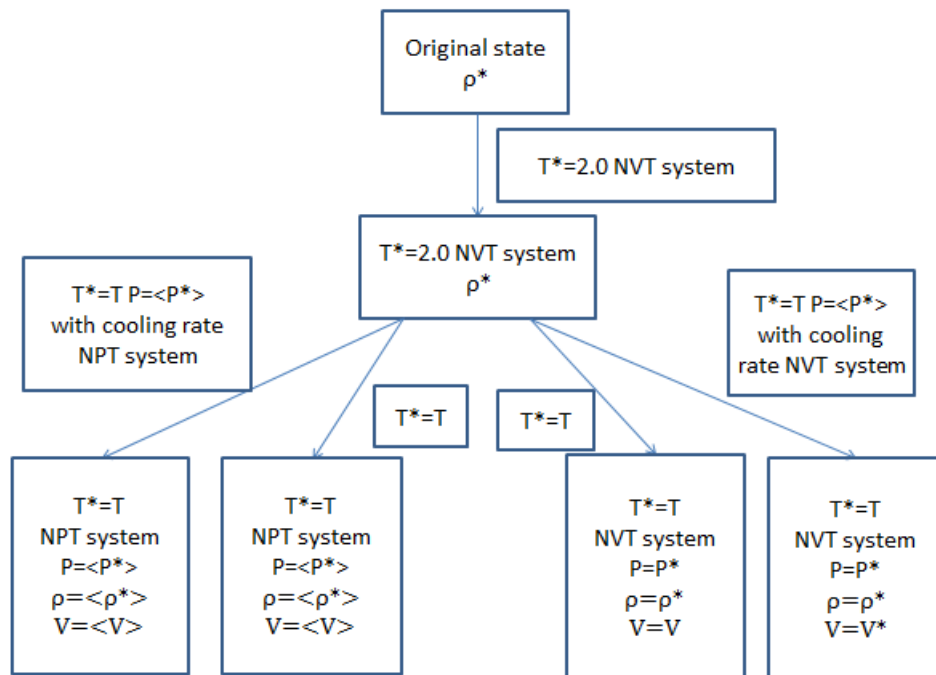


Figure 12. Process of both NVT and NPT system, each system also compared with different cooling rates.

Chapter 4 Conclusion

In conclusion, we have studied 2D-dimensional dimers in colloidal system with a hybrid Lennard-Jones and Yukawa potential. The model accounts for particles interaction through the short-range attraction that leads to dimer aggregation or cluster formation and long-range repulsion which maintains cluster stabilization. Extensive molecular dynamics simulations were performed over wide range of temperature and density to ascertain the 2D structures and phases formed by the dimers. The system is found to undergo several structural transitions and exhibit dynamic arrested states at low temperatures and high density. The structural patterns formed include disordered loose clusters, one-dimensional clusters and percolating gel phase. The dimers have a tendency to form staggered arrangements since such structures correspond to favorable minimum energy states. We find that at the fixed density, as temperature decreases, the structure varies from a disordered to an ordered arrangement, and for certain temperature, when density increases the system shows a transition from finite-size aggregates to some one-dimensional clusters and finally reach an arrested percolating gel phase.

By analyzing the configurational structures of system, we have identified a wide range of structural phases including: (i) disordered non-aggregating state, (ii) aggregated state containing small loose clusters, (iii) well-ordered dimers in filament-like clusters, (iv) percolating gel phase, and (v) low density hexagonal lattice of small cluster at low temperature. Some of these transitions were also evidenced in the heat capacity peaks. In addition to these structural phases, we have examined the diffusional behavior of the dimers at different temperature and density. Through careful analysis of the mean square displacement of the dimers versus time, we were

able to identify the region in the thermodynamic phase space where the dimers cease to follow Fickian diffusion, allowing us to identify when the dimers are dynamically arrested. We successfully summarize these results on a temperature-density phase diagram illustrated in Figure 10.

The results obtained in this research have provided fundamental scientific insights and shed light on the behavior of non-spherical colloidal dimers on a planar surface. These results could aid experimentalists to design colloidal dimers to build 2D structures and patterns that are relevant to technological applications in photonics, biomaterials, catalytic supports, and advanced materials.

APPENDIX

Table 3. The analysis of radial distribution function of $g_{aa}(r)$ and $g_{mm}(r)$.

Density=0.204			
T	$g_{aa}(r)$	$g_{mm}(r)$	Feature
0.5	First peak at R=1.15 One peak at R=2.15	First peak at R=1.15 Second peak at R=1.5 Small Third peak at R=2.15	No specific structure
0.3	First peak at R=1.15 One peak at R=2.15 Emergence of the shoulder at R=1.85	First peak at R=1.15 Second peak at R=1.5 Small Third peak at R=2.15	No specific structure
0.2	First peak at R=1.15 One peak at R=2.15 Emergence of the shoulder at R=1.85	First peak at R=1.15 Second peak at R=1.5 Start to show distinctly the third peak at R=2.0 instead of R=2.15	No specific structure
0.15	First peak at R=1.15 One peak at R=2.15 Double peak at R=1.85 and R=2.15	First peak at R=1.15 Second peak at R=1.5 Third peak at R=2.0	Start to form small finite-size aggregates
0.1	First peak at R=1.15 Double peak at R=1.85 and R=2.15 All of these peak become huger than high temperature	First peak at R=1.15 Second peak at R=1.5 Emergence of the peak at R=1.7 R=2.0 becomes the fourth peak	Most of the dimers are formed specific small finite-size aggregates
0.08	First peak at R=1.15 Triple peak at R=1.85, R=2.15 and R=2.3	First peak at R=1.15 Second peak at R=1.5 Third peak at R=1.7 Fourth peak at R=2.0 Fifth peak at R=2.35 Sixth peak at R=2.65	All dimers have already formed specific small finite-size aggregates
0.07	First peak at R=1.15 One peak at R=2.15 Triple peak at R=1.85, R=2.15 and R=2.3	First peak at R=1.15 Second peak at R=1.5 Third peak at R=1.7 Fourth peak at R=2.0 Fifth peak at R=2.35 Sixth peak at R=2.65	All dimers have already formed specific small finite-size aggregates
0.045	First peak at R=1.15 One peak at R=2.15 Huge Triple peak at R=1.85, R=2.15 and R=2.3 Another triple peak at R=2.95, R=3.2 and R=3.5	First peak at R=1.15 Second peak at R=1.5 Third peak at R=1.7 Fourth peak at R=2.0 Fifth peak at R=2.35 Sixth peak at R=2.65 Seventh peak at R=3.5	small finite-size aggregates and one-dimensional long clusters

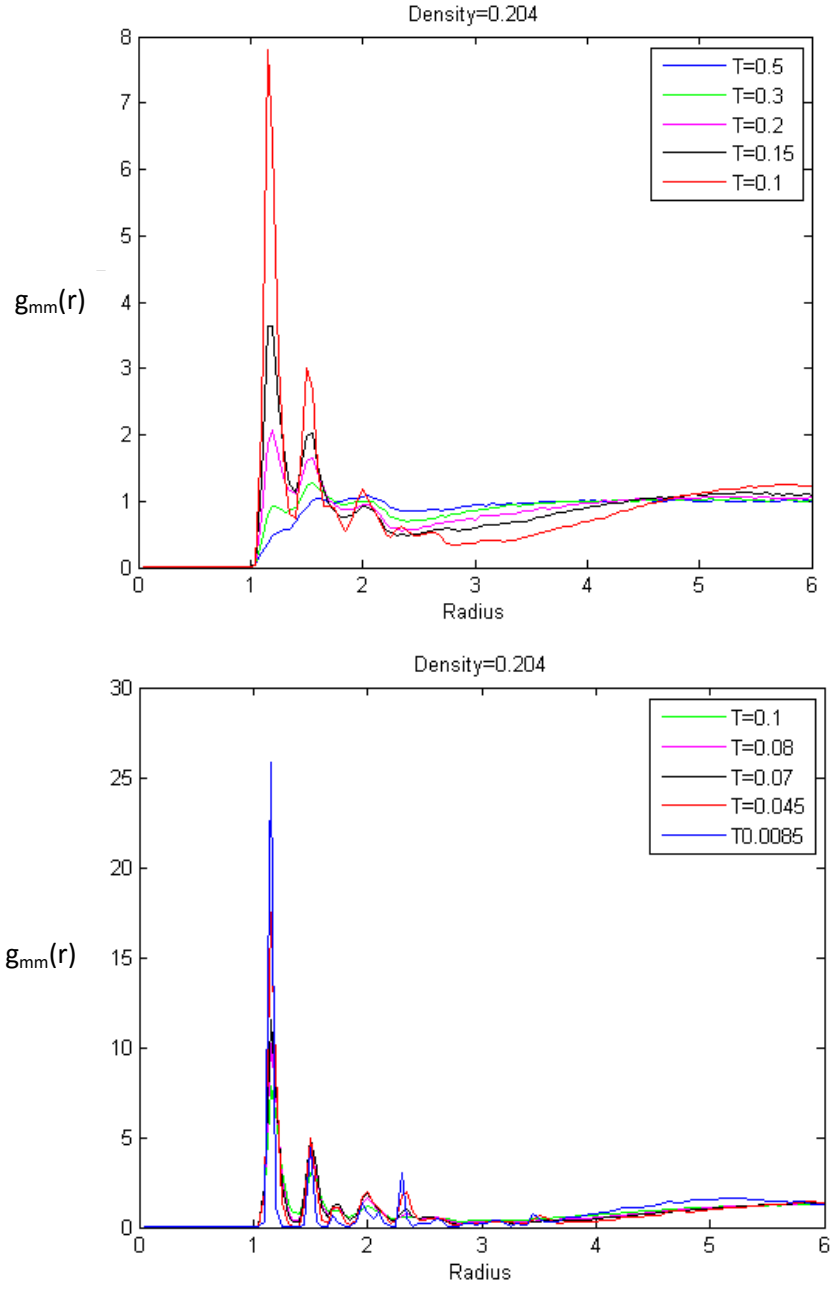


Figure 13. Radial distribution functions $g_{mm}(r)$ for the distance between dimers at wide temperature range $T^* = 0.5 - 0.0085$ at density $\rho^* = 0.204$.

REFERENCES

- [1] M. Seul and D. Andelman, *Science* **267**, 476 (1995).
- [2] A. D. Stoycheva and S. J. Singer, *Phys. Rev. Lett.* **84**, 4657 (2000).
- [3] Gianpietro Malescio and Giuseppe Pellicane, *Phys. Rev. E.* **70**, 021202 (2004).
- [4] G. Malescio and G. Pellicane, *Nat. Mater.* **2**, 97 (2003)
- [5] M. Singh, H. Liu, S. K. Kumar, A. Ganguly and C. Chakravarty, *J. Chem. Phys.* **132**, 074503 (2010).
- [6] Julia Fornleitner and Gerhard Kahl, *J. Phys: Condens. Matter* **22**, 104118 (2010).
- [7] K. J. Strandburg, *Rev. Mod. Phys.* **60**, 161 (1998).
- [8] M. E. Cates, J. P. Wittmer, J. -P Bouchaud, and P. Claudin, *Phys. Rev. Lett.* **81**, 1841 (1998).
- [9] A. Liu and S. Nagel, *Nature (London)* **396**, 12 (1998).
- [10] C. S. O'Hern, L. E. Silbert, A. J. Liu, and S. R. Nagel, *Phys. Rev. E* **68**, 011306 (2003).
- [11] G. Adam and J. H. Gibbs, *J. Chem. Phys.* **43**, 139 (1965).
- [12] M. Ediger, C. Angell, and S. Nagel, *J. Phys. Chem.* **100**, 13200 (1996).
- [13] P. G. Debenedetti and F. H. Stillinger, *Nature (London)* **410**, 259 (2001).
- [14] J. A. Cuesta and D. Frenkel, *Phys. Rev. A* **42**, 2126 (1990).
- [15] I. C. Rankenburg and R. J. Zieve, *Phys. Rev. E* **63**, 061303 (2001).
- [16] T. Schilling, S. Pronk, B. Mulder, and D. Frenkel, *Phys. Rev. E* **71**, 036138 (2005).
- [17] Roel P. A. Dullens, Maurice C. D Mourad, Dirk G. A. L. Aarts, J. P. Hoogenboom, and W. K. Kegel, *Phys. Rev. Lett.* **96**, 028304 (2006).
- [18] L. Filion and M. Dijkstra, *Phys. Rev. E* **79**, 046714 (2009).
- [19] K. Zhao and T. G. Mason, *Phys. Rev. Lett.* **103**, 208302 (2009).
- [20] C. F. Schreck, N. Xu, and C. S. O'Hern, *Soft Matter* **6**, 2960 (2010).
- [21] K. Zhao, R. Bruinsma, and T. Mason, *Proc. Natl. Acad. Sci. USA* **108**, 2684 (2011).

- [22] T. Shen, C. Schreck, B. Chakraborty, D. E. Freed, and C. S. O'Hern, *Phys. Rev. E* **86**, 041303 (2012).
- [23] Y. Han and M. W. Kim, *Soft Matter* **8**, 9045 (2012).
- [24] Y. Han, J. Lee, S. Q. Choi, M. C. Choi, and Mahnn won Kim, *Phys. Rev. E* **88**, 042202 (2013).
- [25] A. B. de Oliveira and M. C. Barbosa, *J. Phys.: Condens. Matter* **17**, 399 (2005).
- [26] A. B. de Oliveira, E. B. Neves, C. Gavazzoni, J. Z. Paukowski, P. A. Netz, and M. C. Barbosa, *J. Chem. Phys.* **132**, 164505 (2010).
- [27] Daniel Salgado-Blanco and Carlos I. Mendoza, *Eur. Phys. J. E.* **36**, 38 (2013).
- [28] K. J. Lee, J. Yoon, J. Lahann, *Curr. Opin. Colloid Interface Sci.* **16**, 195 (2011).
- [29] J. C. F. Toledano, F. Sciortino and E. Zaccarelli, *Soft Matter*, **5**, 2390 (2009).
- [30] W. C. K. Poon, *Curr. Opin. Colloid Interface Sci.*, **3**, 593 (1999).
- [31] V. Trappe and P. Sandkühler, *Curr. Opin. Colloid Interface Sci.*, **8**, 494-500 (2004).
- [32] L. Cipelletti and L. Ramos, *J. Phys.: Condens Matter*, **17**, 253 (2005).
- [33] E. Zaccarelli, *J. Phys.: Condens Matter*, **19**, 323101 (2007).
- [34] A. M. Puertas and M. Fuchs, e-ptint condmat/0810.0681 (2008).
- [35] P. J. Lu, E. Zaccarelli, F. Ciulla, A. B. Schofield, F. Sciortino and D. A. Weitz, *Nature*, **453**, 499 (2008).
- [36] P. Charbonneau and D. R. Reichman, *Phys. Rev. E*, **75**, 011507 (2007).
- [37] D. Pini, J. L. Ge, A. parola and L. Reatto, *Chem. Phys. Lett*, **327**, 209 (2000).
- [38] A.I. Campbell, V. J. Anderson, J. van Duijneveldt and P. Bartlett, *Phys. Rev. Lett*, **94**, 208301 (2005).
- [39] F. Sciortino, P. Tartaglia and E. Zaccarelli, *J. Phys. Chem. B*, **109**, 21942 (2005).
- [40] J. Wu and J. Cao, *Physica A*, **371**, 249 (2006).
- [41] A. de Candia, E. Del Gado, A. Fierro, N Sator, M. Tarzia and A. Coniglio, *Phys. Rev. E*, **74**, 010403 (2006).